

Evaluation of the impact of carotid artery bifurcation angle on hemodynamics by use of computational fluid dynamics: a simulation and volunteer study

Tatsunori Saho^{1,2} · Hideo Onishi²

Received: 14 January 2016/Revised: 17 May 2016/Accepted: 19 May 2016/Published online: 2 June 2016
© Japanese Society of Radiological Technology and Japan Society of Medical Physics 2016

Abstract In this study, we evaluated the hemodynamics of carotid artery bifurcation with various geometries using simulated and volunteer models based on magnetic resonance imaging (MRI). Computational fluid dynamics (CFD) was analyzed by use of OpenFOAM. The velocity distribution, streamline, and wall shear stress (WSS) were evaluated in a simulated model with known bifurcation angles (30°, 40°, 50°, 60°, derived from patients' data) and in three-dimensional (3D) healthy volunteer models. Separated flow was observed at the outer side of the bifurcation, and large bifurcation models represented upstream transfer of the point. Local WSS values at the outer bifurcation [both simulated (<30 Pa) and volunteer (<50 Pa) models] were lower than those in the inner region (>100 Pa). The bifurcation angle had a significant negative correlation with the WSS value ($p < 0.05$). The results of this study show that the carotid artery bifurcation angle is related to the WSS value. This suggests that hemodynamic stress can be estimated based on the carotid artery geometry. The construction of a clinical database for estimation of developing atherosclerosis is warranted.

Keywords Computational fluid dynamics · Pulsatile flow · Carotid artery bifurcation angle · Wall shear stress · Atherosclerosis

1 Introduction

Atherosclerosis is a systemic disease that may develop at a variety of sites [1]. Focal cases tend to develop near the carotid artery bifurcation, leading to the widely accepted idea that hemodynamic forces, i.e., wall shear stress (WSS), play an important role in the development and progression of atherosclerosis [2–4]. Therefore, the carotid artery bifurcation was evaluated for the risk of arteriosclerotic diseases based on the height of its characteristic shape and the frequency of development of arteriosclerosis [5].

In previous studies, arteriosclerosis had been reported to be related to several medical factors, including hemodynamic stresses [6–8]. At the innermost layer of the arterial wall, vascular endothelial cells are directly exposed to hemodynamic forces. WSS is typical; it has been evaluated in previous works. Previous research on endothelial responses to flow had focused on the physiological baseline values of straight arterial segments (1.5–3.0 Pa), or those with relatively low WSS (0.1–0.5 Pa) [7, 9, 10]. The developing factor of atherosclerosis was reset by high shear stress for the systolic phase [1]. These values are relevant to atherogenesis, which tends to occur in low-flow regions that experience disturbed flow or flow recirculation and reattachment.

In recent years, with the development of numerical computation techniques, a number of simulation studies have been reported. In particular, distributions of specific stresses determined by use of computational fluid dynamics

✉ Tatsunori Saho
sahotatsu@gmail.com

Hideo Onishi
onisi@pu-hiroshima.ac.jp

¹ Department of Radiological Technology, Kokura Memorial Hospital, 3-2-1, Asano Kitakyusyu, Fukuoka 802-8555, Japan

² Program in Biological System Sciences, Graduate School of Comprehensive Scientific Research, Prefectural University of Hiroshima, 1-1, Gakuenmachi Mihra, Hiroshima 723-0053, Japan

(CFD) techniques have reproduced the characteristic hemodynamics of the carotid artery bifurcation. These characteristic hemodynamics features were indicated to be risk factors of arteriosclerotic diseases. In previous studies, Lee et al. [5] and Sitzler et al. [11] reported that the development of arteriosclerosis of the carotid artery bifurcation was affected by the tortuosity and angle of distal blood vessels. Additionally, Markl et al. [12] reported on the distribution of WSS and the oscillatory shear index (OSI) in the carotid artery bifurcation. The OSI is an index that is calculated from the temporal variation of the WSS. In these reports, the relationship of atherosclerosis and hemodynamics was evaluated by use of a parameter that indicates the WSS.

Most of these previous hemodynamic studies were based on volunteer models. Evaluation of the volunteer model was patient-specific; the reliability was sufficient for individual patients [13–15]. Moreover, these studies revealed that the specific stress distribution and atherosclerosis are related. The WSS distribution of the carotid artery bifurcation for CFD analysis is greatly affected by the shape of the analysis model. Therefore, local WSS may be predicted based on the shape of the bifurcation. Previous works evaluated the correlation between arteriosclerosis and vascular shape or hemodynamic stress.

This study was based on the relationship between low WSS and atherosclerosis. The relationship between the bifurcation angle and shear stress was considered to be derived by regression to evaluate the changes in the local shear stress due to the vessel bifurcation angle. We believe that high shear stress in the systolic phase might be a significant factor in the development of atherosclerosis. In the present study, we reproduced the bifurcation angle at the carotid artery bifurcation in a simulated model, and we evaluated stress based on the hemodynamic characteristics. Furthermore, each segmented region of the carotid artery bifurcation was evaluated and compared between healthy volunteers. The aim in this study was to evaluate the hemodynamics that was obtained from the simulated model and the volunteer model during the systolic phase, and to examine the possibility of WSS as estimated from the vessel bifurcation angles.

2 Materials and methods

2.1 Study design

The bifurcation angles of the simulated model were determined from data on 50 patients as a preliminary experiment (described in Sect. “2.2”). The bifurcation

angle (α) was defined as the angle between two straight lines passing through the common carotid artery (CCA) and the internal carotid artery (ICA), or through the CCA and the external carotid artery (ECA) of the centroid (Fig. 1). In addition, the carotid artery bifurcation shape for the volunteer models was reconstructed using magnetic resonance imaging (MRI). The number of data used in the volunteer study was 28 (both sides of the carotid artery in 14 subjects). Simulated models and volunteer models were represented by pulsatile blood flow using CFD. The variation in velocity, streamline, and the relationship between WSS and the bifurcation geometry were evaluated at 6 segments of the carotid artery bifurcation. Details of the imaging and lumen reconstruction, as well as the definition and extraction of these sections, were provided elsewhere.

2.2 Participants

The basic data on the simulated models were obtained from 50 consecutive patients who underwent MRI at our facility in October–December 2014 (28 males, 22 females; average age, 73.5 ± 4.6 years). The patient backgrounds are shown in Table 1. Data of the volunteer models were obtained from 14 healthy adult volunteers (5 males, 9 females; average age, 27.3 ± 4.8 years). This was a retrospective and volunteer study, which was approved by our institutional ethical review committee of clinical research.

2.3 Magnetic resonance imaging acquisition

Vascular shapes were obtained by use of Signa HDxt 1.5T (GE healthcare, Milwaukee, USA). Carotid artery shapes were obtained by use of 3D time-of-flight magnetic resonance angiography (3D TOF-MRA). MRI has the potential to assess both vascular geometry and time-resolved 3-directional blood flow with high accuracy *in vivo* [14].

The 3D TOF-MRA imaging parameters were as follows: flip angle, 20° ; echo time/repetition time, 6.9/27 ms; 320×160 matrix; field of view, 24×24 cm; slab thickness, 10 cm; slice thickness, 1.0 mm; number of excitations, 1. Two-dimensional cine phase-contrast MRI (2D cine PC-MRI) provided the inlet profile; it was acquired in the axial cross-section of the common carotid artery of the volunteers. The 2D cine PC-MRI parameters were as follows: flip angle, 20° ; echo time/repetition time, 3.5/6.9 ms; velocity encoding, 120 cm/s; 128×128 matrix; field of view, 29×29 cm; slice thickness, 5.0 mm; number of excitations, 1; views per segment, 4; image acquisition step per one cardiac cycle, 20 steps. CCA flow velocity measurements were performed using Cardiac VX (Advantage Workstation ver. 4. 5, GE healthcare, Milwaukee, WI, USA).

Fig. 1 Representative normal carotid artery bifurcation, showing balance for axial of vessel and the lines through the balance. The bifurcation angle (α) is made by two straight lines **a** The straight line passing through the balance of axial of the CCA and ECA, **b** the straight line passing through the balance of axial of the CCA and ICA

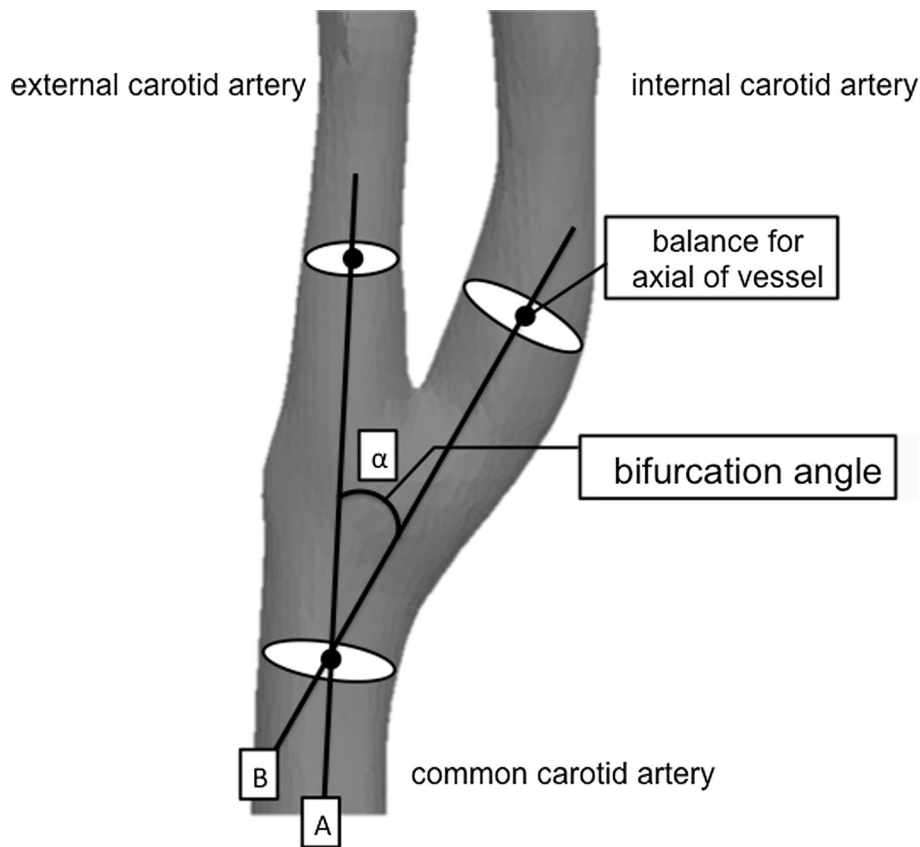


Table 1 Patient population

Disease	Number of examinations
Atherosclerosis	25
Cerebral aneurysm	13
Cerebral tumor	8
Others	4

2.4 Carotid artery bifurcation angles for simulated and volunteer models

The simulated model was created based on the average bifurcation angle of the 50 patients’ data. The average of the all subjects’ (right and left carotid artery, the 100 geometries) bifurcation angle measurement was $41.6 \pm 5.2^\circ$. Therefore, the bifurcation angles of the simulated model were changed (only ICA geometry) from 30 to 60° in increments of 10° (Fig. 2, CCA: $8\text{ mm}\phi$, ICA: $6\text{ mm}\phi$, ECA: $5\text{ mm}\phi$) [8]. Although the bifurcation angle of the ICA has many variations, ECA did not vary as much. Furthermore, it was easy to create the models by changing the angle of one vessel. We changed the geometry of only the ICA in this study. The bifurcation angles of the volunteer models were measured similarly. Volunteer images obtained by MRI were converted into stereolithography

(STL) format following surface rendering in Osirix (Osirix Foundation). The models created were evaluated at 6 characteristic regions, in Fig. 3 (CCA, dividing wall, outer ICA, inner ICA, outer ECA, and inner ECA).

2.5 Computational fluid dynamics

CFD simulations were performed on carotid artery bifurcation geometries derived from the MRI of the 14 volunteer and 4 simulated models. Hexahedral-element meshes were generated using an open source mesh generator (blockMesh, snappyHexMesh; OpenFOAM, Open CFD Ltd., Bracknell, UK) with the use of a uniform node spacing of 0.3 mm , which had previously been shown to be sufficient for resolving WSSs [16]. Fully developed velocity boundary conditions were imposed at the CCA inlet. A rigid wall, a constant blood viscosity of $4.0 \times 10^{-3}\text{ Pa s}$, and a blood density of 1050 kg/m^3 were assumed. Pulsatile hemodynamics was simulated for each carotid artery bifurcation geometry by use of a well-validated finite-volume based CFD solver (OpenFOAM).

Blood flow in the carotid artery had a mean Reynolds number of below 2000. The critical Reynolds number for transition from laminar to turbulent flow is reported to be around 2500; the flows in this study were classified as

Fig. 2 Diagrams showing variable angles of the carotid artery bifurcation, including 30°–60°. The bifurcation angles were derived from patient 3D TOF-MRA data. The created models' ECA angles were fixed at 20°, and ICA angles were changed by 10° (from 10° to 40°)

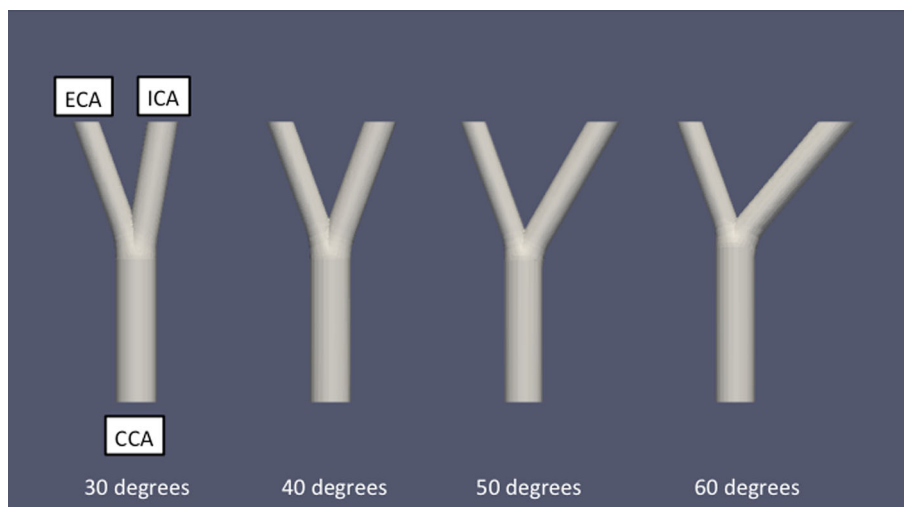
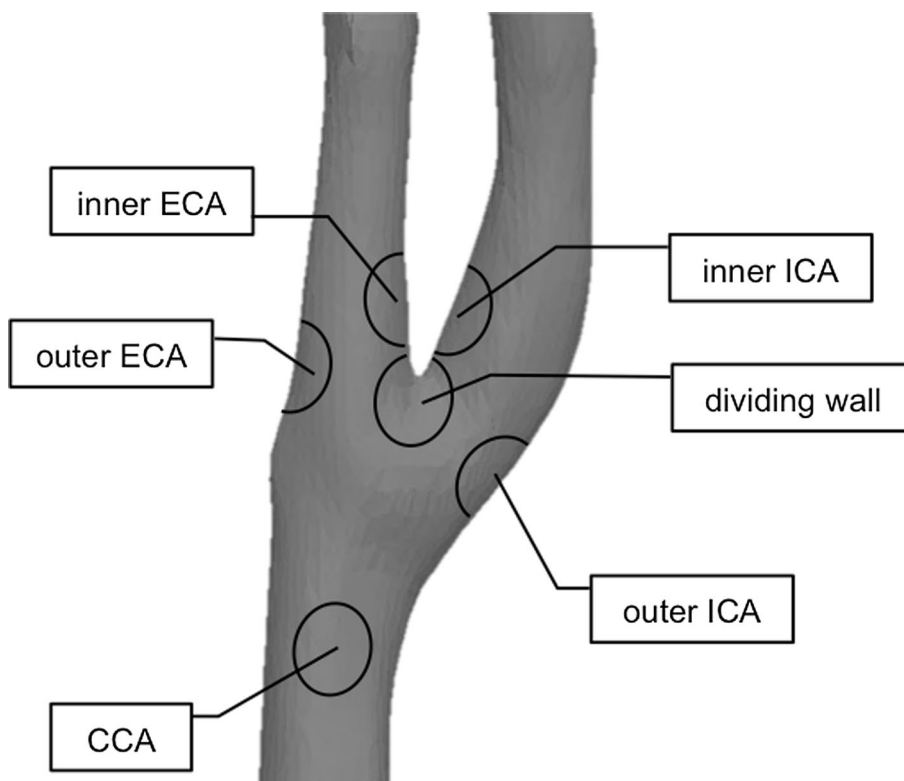


Fig. 3 Scheme of carotid artery segmentation (CCA, dividing wall, outer ICA, inner ICA, outer ECA, and inner ECA)



laminar flow [17]. In the present work, blood was assumed to be a Newtonian and incompressible fluid. The inlet flow condition at the CCA was derived by 2D cine PC-MRI velocity measurement, which was the average value of the flow velocity. The pressure in the outlet conditions at the infinity end was assumed to be 0 Pa. In this study, the aim was to evaluate the hemodynamics of the carotid artery bifurcation at various angles; therefore, patient-specific inlet flow conditions were not used.

2.6 Evaluation

2.6.1 Velocity distribution and streamline

The blood velocity distribution, streamline, and WSS for each model were visualized by Paraview (Kitware Inc., New York, NY, USA). The results were evaluated for the systolic phase. In this study, the blood velocity distributions and streamline were investigated visually for 30°–60°

models (at the CCA, bifurcation, ECA, and ICA). The streamline was a set of velocity vectors that evaluated separated flow and vortex flow, visually.

2.6.2 Wall shear stress

The WSS value calculated by Eq. (1) was applied to the simulation and volunteer models, which were evaluated during the systolic and diastolic phases, where $\vec{\tau}$: WSS (Pa), μ : viscosity (Pa s), \vec{u} : velocity for parallel with wall (m/s), and z : the distance from the wall (m). The WSS distribution was visualized using Paraview. The correlation between the WSS (systolic phase, averaged by local segment) and bifurcation angle was evaluated at 6 segments. In this study, the WSS value derived from the simulated model was defined as WSS_s , whereas the value derived from the volunteer model was defined as WSS_v .

$$\vec{\tau} = \mu \times \frac{\Delta \vec{u}}{\Delta z} \quad (1)$$

2.7 Statistical analysis

The overall quality of the regression was assessed with Spearman's rank correlation coefficient. The contribution of the carotid artery bifurcation angle was determined from the correlation coefficient r . These analyses were performed for the carotid artery bifurcation angle as a test for the sensitivity of our findings in detecting low shear stress.

3 Results

3.1 Velocity measurement for the common carotid artery

The carotid artery flow velocity waveform obtained by 2D cine PC-MRI is shown in Fig. 4. The average heart rate of the subjects was 60.4 beats per min. The plot in Fig. 4 shows an average value of the measurements in each cardiac phase for all subjects. The flow velocity varied with time, and the period of a pulse was roughly 1 s. The flow waveform had a single peak; the maximum value was 69.7 cm/s in systole, and the minimum value was 27.1 cm/s in end-diastole.

3.2 Carotid artery bifurcation angle for the volunteer model

The measured carotid artery bifurcation angle of the volunteers was $35.4^\circ \pm 11.7^\circ$ in male and $42.1^\circ \pm 7.7^\circ$ in female subjects. The carotid bifurcation angle for the female subjects tended to be larger than that of the male

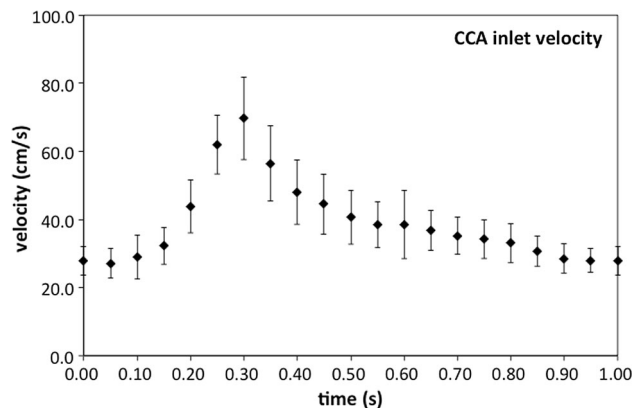


Fig. 4 Velocity waveform shows mean flow obtained from all volunteer data through the common carotid artery during one cardiac cycle. The maximum flow velocity was 69.7 cm/s, determined in the systolic phase. The error bars represent standard deviation

subjects, although the difference was not significant (Welch's t test, p value > 0.05).

3.3 CFD analysis for simulated models

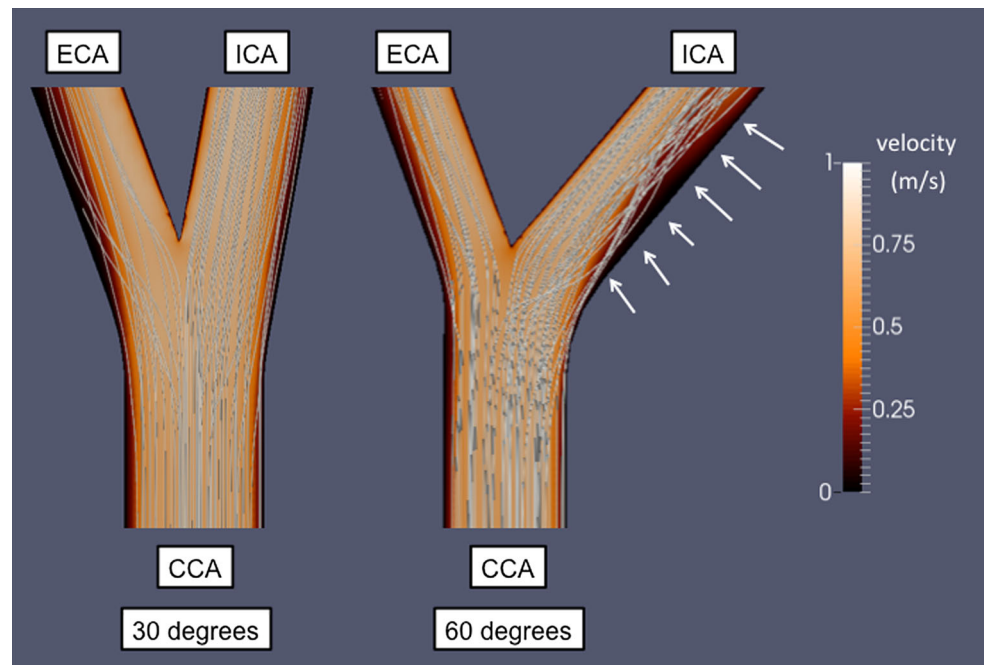
CFD analyses for the simulated models were performed by use of OpenFOAM. The solving time for each bifurcation model was approximately 5 h. The streamline and velocity distribution for the 30° – 60° models are presented in Fig. 5 (systolic phase). For the 30° model, the streamlines along the wall surface were reproduced; the flow rate reduction in the bifurcation was small as compared to the 60° model. For the 60° model, the separated flow was represented at the inner ICA region (Fig. 5, white arrows).

The estimated WSS values derived from the simulated models were shown in Fig. 6 (dotted line). The regression formula, correlation coefficient r , and p values are shown in Table 2. The WSS values for the simulated models indicated a significant strong negative correlation with the bifurcation angle ($0.9 < r$, $p < 0.05$). In particular, the inner region of the carotid artery (dividing wall, inner ICA, inner ECA) showed high WSS values (>100 Pa) for the 30° geometry, whereas the CCA and the outer region (outer ICA, outer ECA) showed low WSS values (<30 Pa) for the same geometry. The WSS reduction by spreading bifurcation angle for the high-WSS region was remarkable as compared to that for the low-WSS region.

3.4 CFD analysis for volunteer models

The volunteer models were also subjected to CFD analysis by use of OpenFOAM. The solving time for each bifurcation model was 5–7 h. The streamline and the velocity distribution for the 25° – 47° models are presented in Fig. 7 (systolic phase). The estimated WSS values derived from

Fig. 5 Visualization of 3D blood flow characteristics and velocity distribution in the carotid artery bifurcation in 30°–60° simulated models. The streamlines were derived by velocity vectors. Separated flow was observed in the outer ICA for the 60° model (*white arrows*). Velocity contour plots at the carotid artery bifurcations for the systolic phase. The scale is in m/s. The wider the bifurcation angle, the lower the velocity in the outer ICA



the volunteer models are shown in Fig. 6 (solid line and scatter plots). The solid line and the scatter plots represent the regression line and measured WSS value for each subject, respectively. The regression formula, correlation coefficient r , and p values are shown in Table 2.

The WSS values of the volunteer models indicated a significant negative correlation with the bifurcation angle ($0.9 < r$, $p < 0.05$). Separated flow was observed at the outer ICA and ECA; thus, the separated flow region was spread for the wide bifurcation model. Disturbed flow was remarkable for the outer ICA (Fig. 7, white arrows), and flow decreasing was wider than outer ECA. A high WSS value (around 150 Pa) was observed in the narrow bifurcation angle models for the inner bifurcation region (dividing wall, inner ICA, inner ECA); both the volunteer and simulated models showed the same tendency. Thus, the low WSS region (< 50 Pa) was distributed in the CCA and the outer side of the bifurcation model (outer ICA, outer ECA). All regions had a moderately negative correlation ($p < 0.05$). The slope of the regression line in the region of the high WSS was up to 7 times higher than that of the regression line of the low WSS (CCA versus inner ECA).

4 Discussion

The evaluation of atherosclerosis with OSI has been reported previously. OSI represents the temporal change in the WSS vector, with low OSI being reported as a risk factor for atherosclerosis. However, previous studies

showed that the atherosclerotic factor was reset in high shear stress during systole [1]. We evaluated the temporal value of WSS during systole.

In previous CFD simulation studies, the carotid bifurcation angle was reported to be correlated with WSS [5, 18]. These reports revealed that changes in the bifurcation shape and WSS values were related; however, they did not consider the variation in the bifurcation angle. In the present study, a significant correlation was observed between the bifurcation angle and WSS in simulated and volunteer models (Fig. 6; Table 2). In particular, a strong correlation between the bifurcation angle and WSS was observed for changes in the bifurcation angle in simulated models, which indicated that the bifurcation angle affected the WSS.

Reduction of the WSS value due to spread of the bifurcation angle was affected by a change in the mainstream direction. The change in mainstream direction shown in Figs. 5 and 7 led to energy loss. The energy loss was causing a secondary flow in a direction perpendicular to the flow direction [4, 19]. This energy loss tended to be stronger for wide bifurcation simulated models in this study, resulting in lower WSS values for wide bifurcation models (Fig. 6). Furthermore, reduction in the WSS value was in effect vortex flow distribution of the local in the bifurcation. The outer ICA region for the volunteer model with wide bifurcation represented strong vortex flow. The same region caused the amount of the WSS values associated with the bifurcation angle to be smaller.

These phenomena were affected by separated flow [18]. The separated flow developed from the lesser curvature of

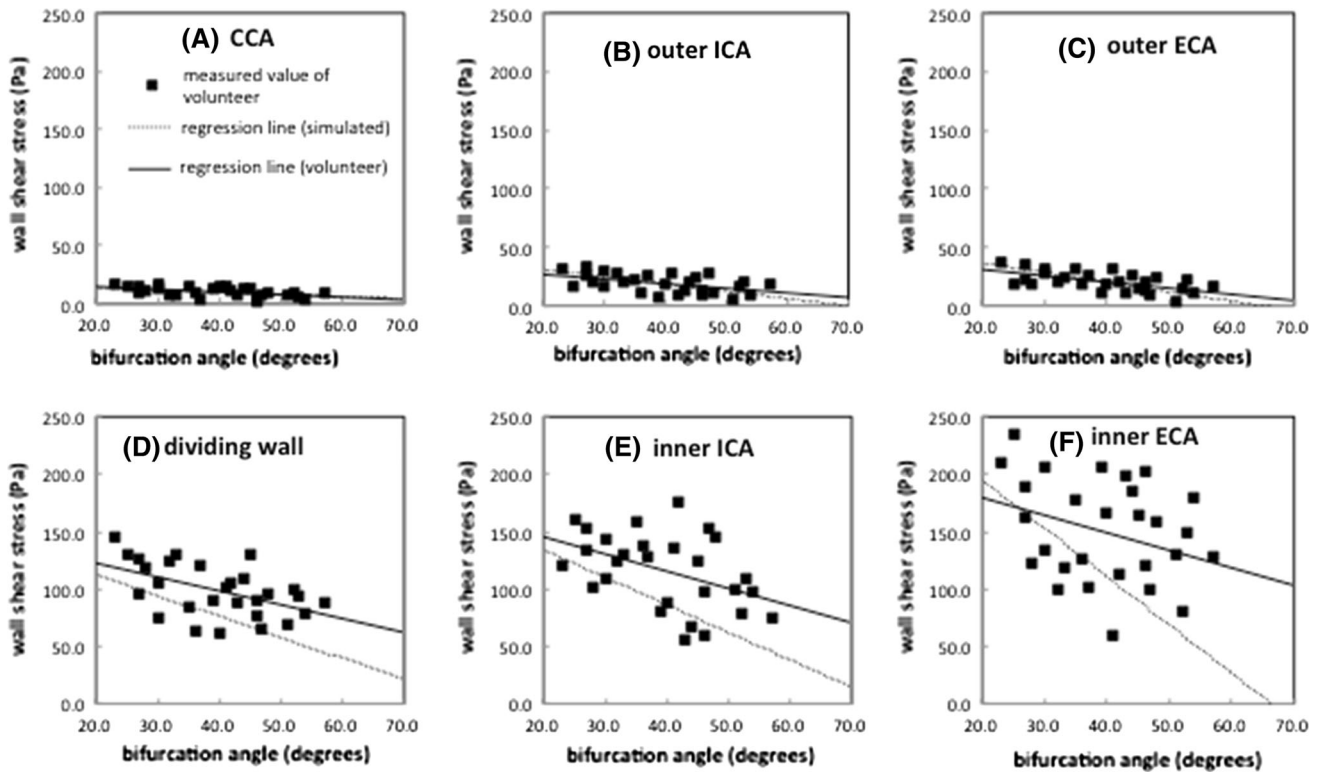


Fig. 6 Wall shear stresses as a function of the bifurcation angle in each segment for simulated (*dotted line*) and volunteer models (*solid line* and *scatter plots*) in the systolic phase. Wall shear stress had a strong negative correlation with the bifurcation angle (in all simulated models). Although the systolic phase had a high flow velocity, the outer ICA, ECA, and CCA regions were exposed to lower shear stress than with the inner ICA, ECA, and dividing wall regions. **a** CCA: the two regression lines (simulated and volunteer) had good agreement for bifurcation angle. **b** Outer ICA: the regression line (simulated) was slightly overestimated for narrow bifurcation angle, and slightly underestimated for wide bifurcation angle. **c** Outer ECA: the two

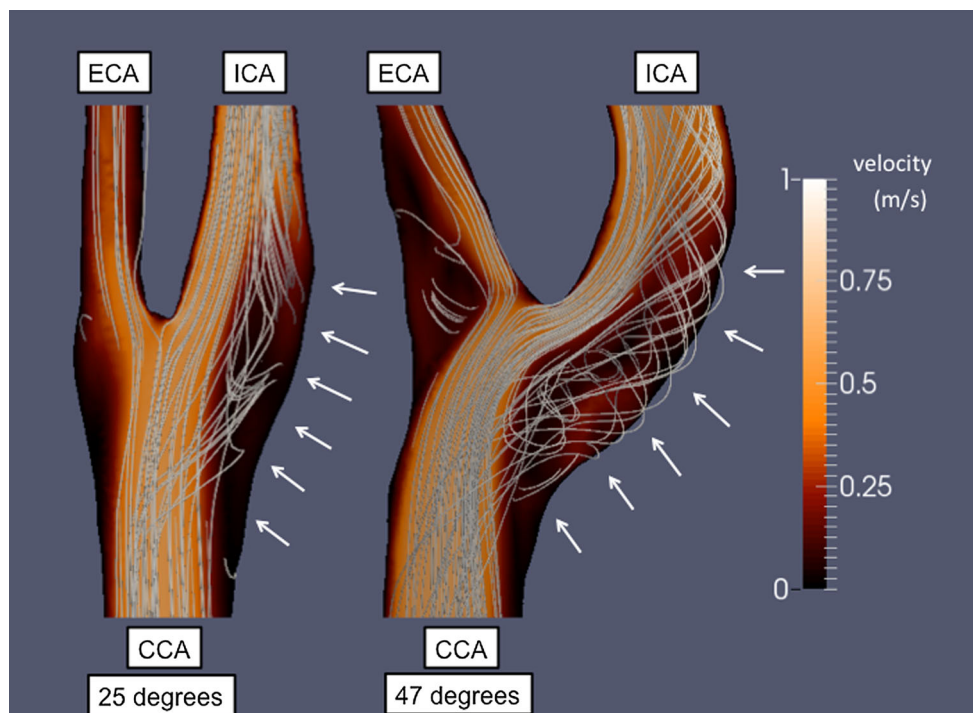
regression lines (simulated and volunteer) had the same tendency for the outer ICA. **d** Dividing wall: the regression line (simulated) was underestimated for volunteer data. This tendency was remarkably observed for the wider bifurcation angle. Furthermore, a narrow bifurcation angle ($\alpha < 30^\circ$) presented a higher WSS value than CCA, outer ICA, and outer ECA. **e** Inner ICA: the regression line (simulated) was underestimated for volunteer data, and indicated the same tendency for the dividing wall. **f** Inner ECA: the two regression lines (simulated and volunteer) differed for a wider bifurcation angle. The estimated WSS value (simulated and volunteer) was highest for all segments

Table 2 The contribution of carotid artery bifurcation angle for each region. Two formulas (WSS_s and WSS_v) represented the regression line derived from the simulated model and the volunteer model of each segment in Fig. 6 (variable α : carotid artery bifurcation angle). Correlation coefficient r represented the extent of correlation between WSS and carotid artery bifurcation angle α

	Regression formula	Correlation coefficient r	p value
CCA	$WSS_s = -0.18\alpha + 16.81$	0.96	0.0006
	$WSS_v = -0.23\alpha + 19.35$	0.55	0.003
Dividing wall	$WSS_s = -1.82\alpha + 148.82$	0.91	0.0002
	$WSS_v = -1.21\alpha + 146.48$	0.51	0.006
Outer ICA	$WSS_s = -0.62\alpha + 42.95$	0.96	0.0004
	$WSS_v = -0.39\alpha + 34.31$	0.49	0.008
Inner ICA	$WSS_s = -1.50\alpha + 175.20$	0.94	0.0001
	$WSS_v = -1.82\alpha + 148.83$	0.44	0.019
Outer ECA	$WSS_s = -0.81\alpha + 52.20$	0.90	0.0004
	$WSS_v = -0.53\alpha + 41.38$	0.61	0.001
Inner ECA	$WSS_s = -4.21\alpha + 279.17$	0.99	0.0004
	$WSS_v = -1.53\alpha + 209.94$	0.42	0.034

α bifurcation angle

Fig. 7 Visualization of 3D blood flow characteristics in the carotid artery bifurcation in volunteer models with narrow (25°) and wide (47°) bifurcation angles. The streamlines were derived by velocity vectors. Separated flow was observed in the outer ICA (white arrows); it was remarkable for wide bifurcation. Velocity contour plots at the carotid artery bifurcations for the systolic phase. The scale is in m/s. Both models showed reduction of velocity in the outer region



the point where the mainstream of direction had changed. As the bifurcation angle spread, the separated flow area developed (Fig. 5, white arrows). Therefore, the outer ICA indicated a low WSS value for the simulated models.

The same phenomenon was observed in the volunteer models (Fig. 7, white arrows). The vortex flow due to separated flow showed more helicity in the outer ICA for the wide bifurcation model. Complication of such vortex and separated flows caused energy loss in the outer ICA, leading to reduction in the flow velocity and WSS. Additionally, although the simulated models showed a strong correlation, the volunteer models showed a moderate correlation (Table 2). This indicated that factors related to other shapes as well the bifurcation angle also contributed to the hemodynamics [4, 19]. Markl et al. reported that tortuosity and vessel diameters affected the WSS [13]. Changes in the vessel diameter affect the blood flow velocity and flow ratio of the ICA and ECA. Additionally, changes in geometry with torsion of the blood vessel affected the occurrence point of the separated flow. These effects could not be ignored in the evaluation of the hemodynamics. However, our findings suggested that the bifurcation angle contributes to the development of separated flow in the carotid artery bifurcation; this was shown to be correlated with changes in the WSS value.

In a previous study, chronic exposure to low WSS reportedly led to the development of arteriosclerosis [2]. In this study, WSS was altered by the bifurcation angle, reduced according to the spread of the bifurcation angle.

Therefore, the area exposed to low WSS can be estimated; the larger the spread of the bifurcation angle exposed to low WSS, the higher the risk of development of atherosclerosis in the future.

In this study, we had made the customary assumptions of a rigid wall, Newtonian fluid, and a fully developed inlet velocity, shown in previous work to be of relatively minor influence on the distribution of WSS [20–22]. Improvement on these limitations will advance hemodynamic evaluations in the future. Another limitation of this study was the vascular configuration of the carotid artery bifurcation. Further investigations will be required before our findings can be extrapolated to other arteries.

5 Conclusions

Simulated and volunteer models for various bifurcation angles were subjected to CFD analysis, and WSS values were evaluated for each segment of the carotid artery bifurcation during the systolic phase. The WSS value of each segment in the bifurcation indicated a significant negative correlation with the carotid artery bifurcation angle. The results of this study suggested that the carotid artery bifurcation angle is related to the WSS value. Furthermore, this work suggests that the hemodynamic stress for the systolic phase can be estimated from the carotid artery geometry. In the future, more clinical data should be evaluated in advance, and the construction of a clinical

database for the estimation of developing atherosclerosis is required.

Acknowledgments This study was supported by the Digital image scientific research conference in Mihara.

Complicance with ethical standards

Conflict of interest The authors declare no conflicts of interest.

References

- Sho E, Sho M, Singh TM, Xu C, Zarins CK, Masuda H. Blood flow decrease induces apoptosis of endothelial cells in previously dilated arteries resulting from chronic high blood flow. *Arter Thromb Vasc Biol.* 2001;21(7):1139–45.
- Kumar V, Cotran SR, Robbins LS. Section10 vascular. Robbins basic pathology. 7th ed. Philadelphia: Elsevier Saunders; 2003. p. 409–54.
- Zhang Y, Furusawa T, Sia SF, Umezu M, Qian Y. Proposition of an outflow boundary approach for carotid artery stenosis CFD simulation. *Comput Method Biomech Biomed Eng.* 2013;16(5):488–94.
- Nguyen KT, Clark CD, Chancellor TJ, Papavassiliou DV. Carotid geometry effects on blood flow and on risk for vascular disease. *J Biomech.* 2008;41(1):11–9.
- Lee SW, Antiga L, Steinman DA. Correlations among indicators of disturbed flow at the normal carotid bifurcation. *J Biomech Eng.* 2009;131(6):061013.
- Saho T, Onishi H. Quantitative comparison of hemodynamics in simulated and 3D angiography models of cerebral aneurysms by use of computational fluid dynamics. *Radiol Phys Technol.* 2015;8(2):258–65.
- Zarins CK, Giddens DP, Bharadvaj BK, Sottiurai VS, Mabon RF, Glagov S. Carotid bifurcation atherosclerosis. Quantitative correlation of plaque localization with flow velocity profiles and wall shear stress. *Circ Res.* 1983;53(4):502–14.
- Saho T, Onishi H, Sugihara T, Nakamura Y, Yuda I. Tackling hemodynamic analysis of the carotid artery using opensource software and computational fluid dynamics. *Nihon Housyasen Gijutsu Gakkai Zasshi.* 2013;69:1241–9.
- Jou LD, van Tyen R, Berger SA, Saloner D. Calculation of the magnetization distribution for fluid flow in curved vessels. *Magn Reson Med.* 1996;35(4):577–84.
- Dolan JM, Meng H, Singh S, Paluch R, Kolega J. High fluid shear stress and spatial shear stress gradients affect endothelial proliferation, survival, and alignment. *Ann Biomed Eng.* 2011;39(6):1620–31.
- Sitzer M, Puac D, Buehler A, Steckel AD, Kegler S, Markus SH, Steinmetz H. Internal carotid artery angle of origin: a novel risk factor for early carotid atherosclerosis. *Stroke.* 2003;34:950–5.
- Markl M, Wegent F, Zech T, Bauer S, Strecker C, Schumacher M, Weiller C, Hennig J, Harloff A. In vivo wall shear stress distribution in the carotid artery effect of bifurcation geometry, internal carotid artery stenosis, and recanalization therapy. *Circ Cardiovasc Imaging.* 2010;3(6):647–55.
- Marshall I, Zhao S, Papathanasopoulou P, Hoskins P, Xu XY. MRI and CFD studies of pulsatile flow in healthy and stenosed carotid bifurcation models. *J Biomech.* 2004;37(5):679–87.
- Papathanasopoulou P, Zhao S, Köhler U, Robertson MB, Long Q, Hoskins P, Xu XY, Marshall I. MRI measurement of time-resolved wall shear stress vectors in a carotid bifurcation model, and comparison with CFD predictions. *J Magn Reson Imaging.* 2003;17(2):153–62.
- Kamenskiy AV, Pipinos II, Dzenis YA, Bikhchandani J, Gupta PK, Phillips N, Kazmi SAJ, MacTaggart JN. Effects of carotid artery stenting on arterial geometry. *J Am Coll Surg.* 2013;217(2):251–62.
- Lee SW, Antiga L, Spence JD, Steinman DA. Geometry of the carotid bifurcation predicts its exposure to disturbed flow. *Stroke.* 2008;39:2341–7.
- Sarpkaya T. Experimental determination of the critical Reynolds number for pulsating Poiseuille flow. *J Fluid Eng.* 1966;88(3):589–98.
- Iaccarino G. Predictions of a turbulent separated flow using commercial CFD codes. *J Fluid Eng.* 2001;123(4):819–28.
- De SD, Franjić BD, Lovričević I, Vukelićand M, Palenkić H. Carotid bifurcation position and branching angle in patients with atherosclerotic carotid disease. *Coll Antropol.* 2005;29(2):627–32.
- Moyle KR, Antiga L, Steinman DA. Inlet conditions for image-based CFD models of the carotid bifurcation: is it reasonable to assume fully developed flow? *J Biomech Eng.* 2006;128(3):371–9.
- Lee SW, Steinman DA. On the relative importance of rheology for image-based CFD models of the carotid bifurcation. *J Biomech Eng.* 2007;129(2):273–8.
- Younis HF, Kaazempur-Mofrad MR, Chan RC, Isasi AG, Hinton DP, Chau AH, Kim LA, Kamm RD. Hemodynamics and wall mechanics in human carotid bifurcation and its consequences for atherogenesis: investigation of inter-individual variation. *Bio-mech Model Mechanobiol.* 2004;3(1):17–32.